available for the analysis of the experimental data. The following information might then be sought [6]:

1) hourly, median, or 10 to 15 minute average values of signal,
2) complete coded sonde data,
3) details of inversion heights,
4) details of constant pressure surfaces,
5) changes in the common volume,
6) identification of large scale weather changes (frontal passages, monsoon effects, etc.).

A. M. J. Mitchell
T. K. Fitzsimons
Signals Res. and Develop. Establishment
Ministry of Technology
Christchurch, Hants., England

References

[1] R. Larsen, "A comparison of some troposcatter prediction methods," Conference on Tropospheric Wave Propagation, IEE (London), Conf. Publ. 48, pp. 110–117, October 1968.
[2] E. W. Anderson, "Tropospheric scatter surveys," *Point to Point Telecomm.*, vol. 12, pp. 4–14, January 1968.
[3] F. A. Gunther, "Tropospheric scatter communications, past, present and future," *IEEE Spectrum*, vol. 3, pp. 79–100, September 1966.
[4] T. K. Fitzsimons, "Observations of tropospheric scatter path loss at C-band frequencies and meteorological conditions in Cyprus," *Proc. IEE* (London), vol. 115, pp. 898–902, July 1968.
[5] L. Boithias, "An experimental study of antenna gain loss," *IEEE Trans. Antennas and Propagation (Communications)*, vol. AP-15, pp. 578–579, July 1967.
[6] C. A. Samson, private communication. ESSA Res. Labs., Boulder, Colo., November 7, 1968.

Correction to "Frequency Correlation of Line-of-Sight Signal Scintillations"

In the above paper[1] using the notation sgn (x) for the sign of x, eqs. (19) and (35)–(41) should read as follows:

$$Q_n(z) = \sqrt{\frac{\pi}{2n}}\,[-i\,\mathrm{sgn}\,(\mathrm{Im}\,z)]^{n+1} \cdot\exp\left[\left(n+\frac{1}{2}\right) iz\,\mathrm{sgn}\,(\mathrm{Im}\,z)\right] \tag{19}$$

$$f(\xi) = \log\left(\frac{1-\xi^2}{z-\xi}\right) \tag{35}$$

$$\xi_0 = z - i\sqrt{1-z^2}\,\mathrm{sgn}\,(\mathrm{Im}\,z)$$
$$\xi_0 \cong z - \mathrm{i}\,\mathrm{sgn}\,(\mathrm{Im}\,z) \tag{36}$$

$$f(\xi) = f(\xi_0) - \frac{(\xi-\xi_0)^2}{2} \cdot[1 - iz\,\mathrm{sgn}\,(\mathrm{Im}\,z)] \tag{37}$$

Manuscript received December 12, 1968.

[1] R. B. Muchmore and A. D. Wheelon, *IEEE Trans. Antennas and Propagation*, vol. AP-11, pp. 46–51, January 1963.

$$Q_n(z) \cong \frac{e^{n\,(\xi_0)}}{2^{n+1}} \int_{-1}^{+1} \frac{d\xi}{z-\xi} \cdot\exp\left[-\frac{1}{2}n(\xi-\xi_0)^2 \cdot(1 - iz\,\mathrm{sgn}\,(\mathrm{Im}\,z))\right]$$
$$\cong \frac{e^{nf(\xi_0)}}{2^{n+1}} \int_{-\infty}^{\infty} \frac{d\xi}{z-\xi} \cdot\exp\left[-\frac{1}{2}n(\xi-\xi_0)^2 \cdot(1 - iz\,\mathrm{sgn}\,(\mathrm{Im}\,z))\right]$$
$$\cong \frac{e^{nf(\xi_0)}}{2^{n+1}} \sqrt{\frac{2\pi}{n}}\,\frac{1}{z-\xi_0} \cdot\frac{1}{\sqrt{1 - iz\,\mathrm{sgn}\,(\mathrm{Im}\,z)}} \tag{38}$$

$$f(\xi_0) = \log\left[\frac{1-\xi_0^2}{z-\xi_0}\right] = \log\left[\frac{2 - z^2 + 2iz\,\mathrm{sgn}\,(\mathrm{Im}\,z)}{i\,\mathrm{sgn}\,(\mathrm{Im}\,z)}\right]$$
$$\cong \log\,[-2i\,\mathrm{sgn}\,(\mathrm{Im}\,z)] + iz\,\mathrm{sgn}\,(\mathrm{Im}\,z) + \cdots \tag{39}$$

$$e^{nf(\xi_0)} \cong [-2i\,\mathrm{sgn}\,(\mathrm{Im}\,z)]^n \cdot\exp\,[inz\,\mathrm{sgn}\,(\mathrm{Im}\,z)] \tag{40}$$

$$Q_n(z) \cong \sqrt{\frac{\pi}{2n}}\,[-i\,\mathrm{sgn}\,(\mathrm{Im}\,z)]^{n+1} \cdot\exp\left[i\left(n+\frac{1}{2}\right) z\,\mathrm{sgn}\,(\mathrm{Im}\,z)\right]. \tag{41}$$

J. A. Karas
Aerospace Group
Hughes Aircraft Co.
Los Angeles, Calif. 90009

Dipole Admittance for Magnetoplasma Diagnostics

***Abstract*—A method is presented for calculating the admittance of a short thin dipole antenna in a cold collisional magnetoplasma. The theory is quasi-static, and the results are slightly more accurate than in previous analyses. Numerical calculations of admittance as a function of frequency are presented for several different orientations of the dipole with respect to the magnetic field. For any orientation the calculations show that the plasma frequency and the upper hybrid frequency can be readily identified.**

In the last few years significant progress has been made in the measurement of rocket-borne antenna admittance for ionosphere plasma diagnostics. Spherical probe [1] and dipole [2] swept-frequency measurements have shown that it is possible by such means to identify the plasma and upper hybrid frequencies in the E and F regions of the ionosphere. From the theoretical point of view, calculations for spherical probes [3] have exhibited encouraging agreement with experiments. This communication presents a set of admittance calculations for a short thin dipole and indicates the extent to which these calculations agree with rocket experiments.

In a previous paper by Balmain [4] it was shown that the following formula represents the uniform-plasma impedance of a thin cylindrical dipole of radius R and half-length L with its axis making an angle θ with the magnetic field:

$$Z = \frac{1}{j\omega\pi\epsilon_0 L'}\left[\ln\frac{L'}{R'} - 1\right] \tag{1}$$

where

$$L' = L\sqrt{K'}\sqrt{T} \tag{2}$$

$$R' = \frac{R}{2}\left(\frac{K'\sqrt{K_0}}{\sqrt{T}} + \sqrt{K'}\sqrt{K_0}\right) \tag{3}$$

$$T = K_0\sin^2\theta + K'\cos^2\theta \tag{4}$$

$$K_0 = 1 - \frac{X}{U}$$

$$K' = 1 - \frac{XU}{U^2 - Y^2}$$

$$X = \frac{\omega_p^2}{\omega^2}$$

$$Y^2 = \frac{\omega_c^2}{\omega^2}$$

$$\omega_u^2 = \omega_p^2 + \omega_c^2$$

ω_p = plasma frequency

ω_c = cyclotron frequency

ω_u = upper hybrid frequency

$$U = 1 - j\frac{\nu}{\omega}$$

ν = collision frequency.

In [4] eq. (70) in its free-space form gives the dipole impedance expression

$$Z(\beta,L) = \frac{F(\beta)}{j\omega\pi\epsilon_0 L} \tag{5}$$

where

$$F(\beta) = \ln\frac{(1+\sqrt{1+\beta^2})^2}{\beta(2+\sqrt{4+\beta^2})} + \tfrac{1}{2}(3\beta + \sqrt{4+\beta^2} - 4\sqrt{1+\beta^2}) \tag{6}$$

$$\beta = \frac{R}{L}. \tag{7}$$

This is slightly more accurate than the free-space form of (1) which is valid only for extremely thin dipoles. Equation (5) can be used for anisotropic plasma calculations by employing the dimensional scaling represented by (2) and (3). In addition, the ion sheath can be taken into account approximately by representing it as a sharply bounded vacuum gap of thickness S. With the definitions

$$\beta_s = \frac{R+S}{L} \tag{8}$$

Manuscript received November 14, 1968.

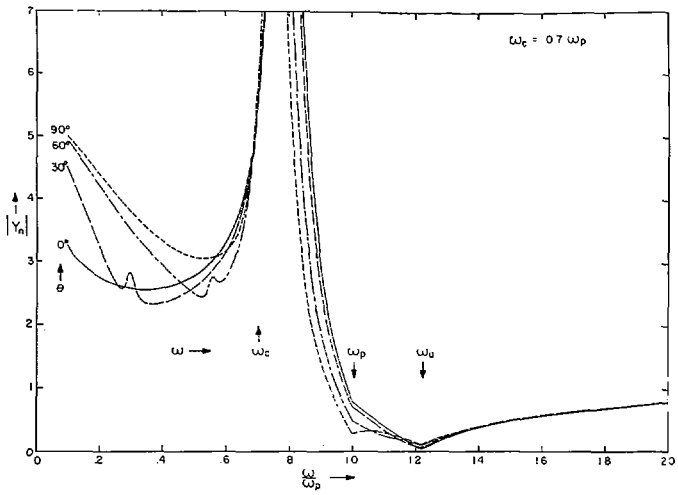

Fig. 1.

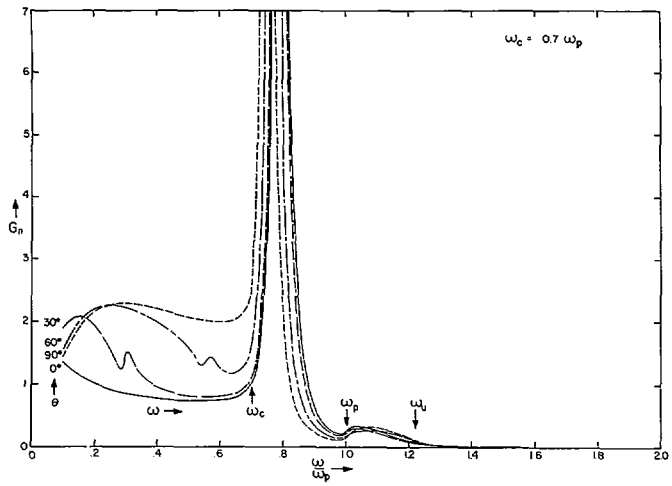

Fig. 4.

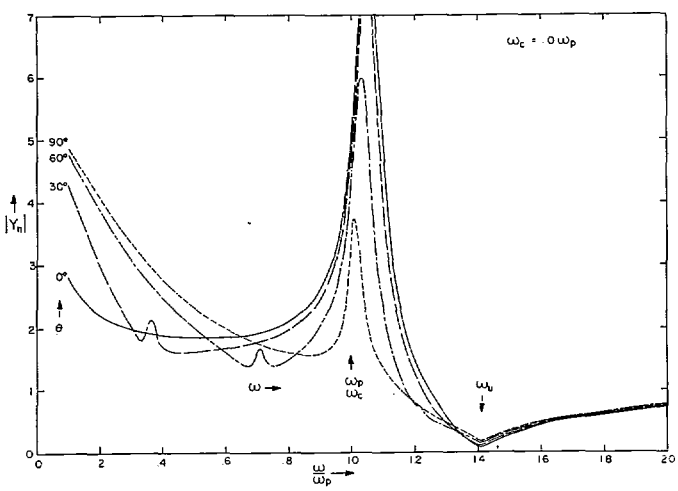

Fig. 2.

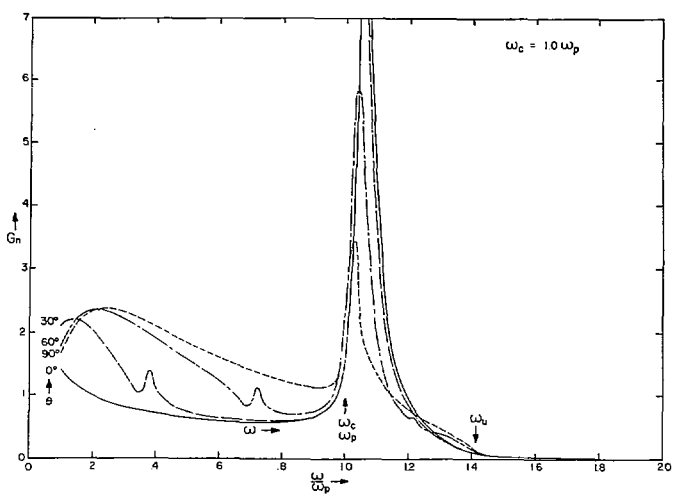

Fig. 5.

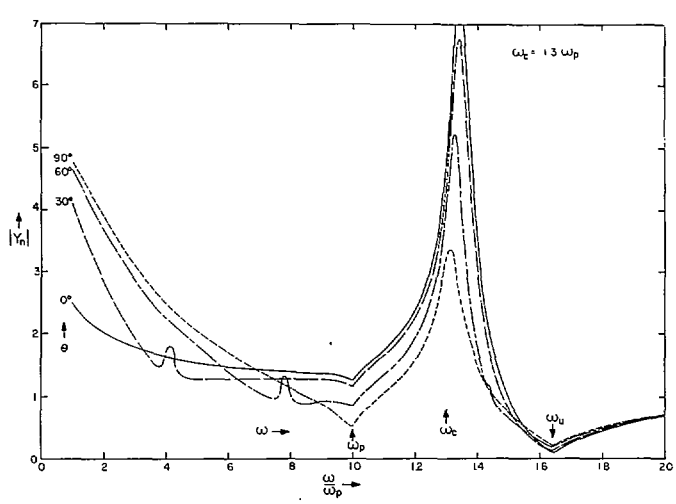

Fig. 3.

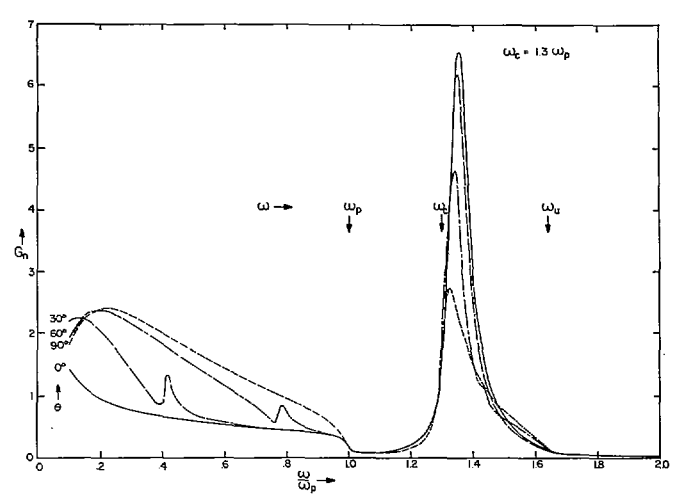

Fig. 6.

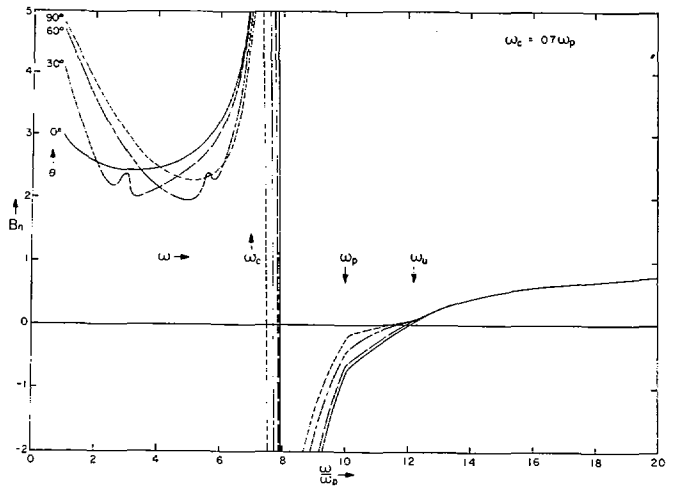

Fig. 7.

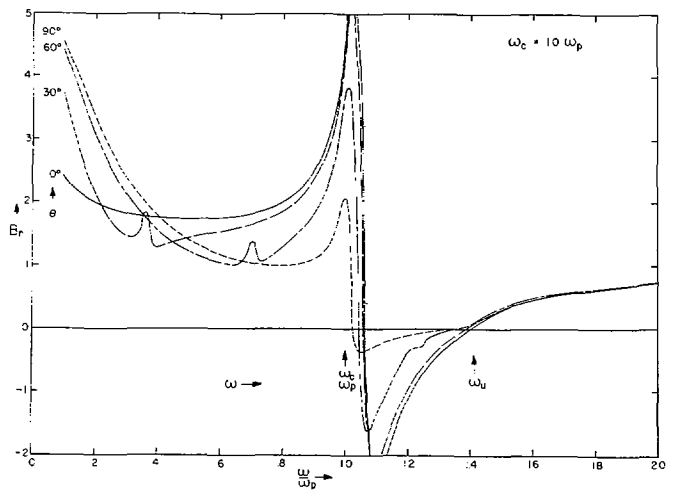

Fig. 8.

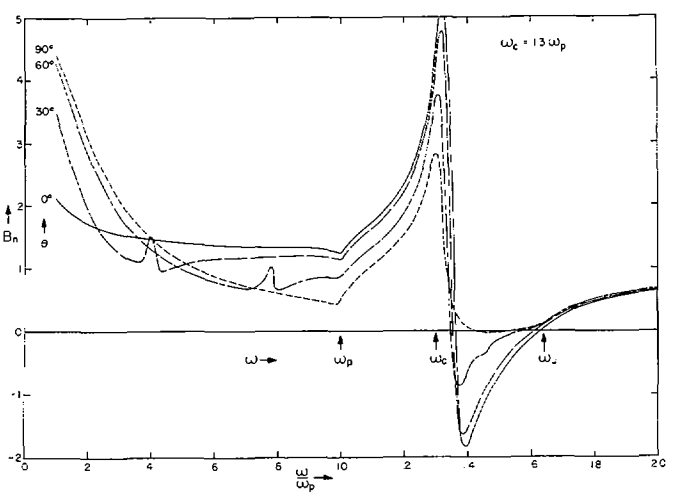

Fig. 9.

$$\beta_p = \frac{R+S}{L}\cdot\frac{\sqrt{K_0}}{2\sqrt{T}}\left(\frac{\sqrt{K'}}{\sqrt{T}}+1\right) \quad (9)$$

it is possible to express the dipole admittance in the following normalized form (so as to make the free-space admittance magnitude equal to unity):

$$Y_n = G_n + jB_n = \frac{|Z_{\text{free space}}|}{Z_{\text{sheath}} + Z_{\text{plasma}}} \quad (10)$$

where

$$Z_{\text{free space}} = Z(\beta, L)$$
$$Z_{\text{sheath}} = Z(\beta, L) - Z(\beta_s, L)$$
$$Z_{\text{plasma}} = Z(\beta_p, L').$$

It follows that

$$Y_n = j\frac{F(\beta)}{F(\beta) - F(\beta_s) + \dfrac{F(\beta_p)}{\sqrt{K'}\sqrt{T}}}. \quad (11)$$

This is the formula used in the numerical calculations for which the following values have been selected: $L = 100$ cm, $R = 1$ cm, $S = 1$ cm, $\nu = 0.02\,\omega_p$. These are suitable to represent a small rocket antenna in the E region of the ionosphere.

The magnitude of the normalized admittance $|Y_n|$ is shown in Figs. 1–3. The high peak is the sheath-plasma "series resonance." The upper hybrid frequency ω_u is identifiable in all three cases, and the plasma frequency is identifiable in Figs. 1 and 3. In these respects the graphs are qualitatively similar to the experimental results of Melzner and Rabben [2]. In addition, in the graphs for $\theta = 30$ and 60 degrees small anomalies are evident when the dipole axis is parallel to the "characteristic cones" described by Balmain [4] (for the lossless case, when $T = 0$). The characteristic-cone anomalies are clearly evident in the low-frequency hyperbolic region ($\omega < \omega_p$ and ω_c) but are almost indistinguishable in the high-frequency hyperbolic region ($\omega > \omega_p$ and ω_c, $\omega < \omega_u$). As far as is known, these anomalies have not been observed experimentally.

The normalized conductance G_n in Figs. 4–6 exhibits the expected peak at the series resonance and is also high in the hyperbolic regions. This is the same sort of behavior as was observed by Heikkila *et al.* [1] in their experiments on a rocket-borne spherical probe.

The normalized susceptance B_n in Figs. 7–9 is qualitatively similar to the measurements of Heikkila *et al.* [1] except, of course, for the characteristic-cone anomalies. At first glance one might think that the zero in susceptance would be useful as an indicator of sheath thickness. In practice this is only partly true because the theory does not account fully for loss processes and inhomogeneity, both of which affect the position of the zero. Furthermore, in Fig. 9 the $\theta = 90$ degree curve shows that at times there will be no definite zero in susceptance.

The most striking feature of all the calculations is their relative insensitivity to changes in orientation angle θ, at least, as far as the overall appearance of the

graphs is concerned. Only the characteristic-cone anomalies depend on θ, and therefore if they could be observed experimentally, they would serve to give the orientation of the antenna relative to the magnetic field. For the purpose of plasma diagnostics it appears that the admittance magnitude is the most useful quantity to measure, because the plasma and upper hybrid frequencies are readily identifiable. Furthermore, at these frequencies the admittance magnitude exhibits minima which, in general, are easier to measure than maxima, especially when saturation of the measuring device or telemetry channel is possible.

Acknowledgment

The author wishes to thank D. F. Parsons for preparing the computer program.

Keith G. Balmain
Dept. of Elec. Engrg.
University of Toronto
Toronto, Ont., Canada

References

[1] W. J. Heikkila, J. A. Fejer, J. Hugill, and W. Calvert, "Comparison of ionospheric probe techniques" in *Space Research*, vol. 7. Amsterdam, The Netherlands: North Holland Publ. Co., pp. 395–406.
[2] F. Melzner and H. H. Rabben, "Electron density measurements in the ionosphere with high altitude rockets" in *Plasma Waves in Space and in the Laboratory*, vol. 2, J. O. Thomas and B. J. Landmark, Eds. Edinburgh, Scotland: Edinburgh University Press, 1969.
[3] K. G. Balmain and G. A. Oksiutik, "RF probe admittance in the ionosphere: theory and experiment" in *Plasma Waves in Space and in the Laboratory*, vol. 1, J. O. Thomas and B. J. Landmark, Eds. Edinburgh, Scotland: Edinburgh University Press, 1969.
[4] K. G. Balmain, "The impedance of a short dipole antenna in a magnetoplasma" *IEEE Trans. Antennas and Propagation*, vol. AP-12, pp. 605–617, September 1964.

Radiation Patterns of a Slot Antenna in the Presence of a Breakdown Sheath

Abstract—The experimental radiation patterns are measured for a 0.4×0.9-inch slot antenna in the presence of aperture breakdown over a wide range of gas pressures and breakdown power levels. It was found that pattern distortion caused by the breakdown plasma was not very significant. The overall signal attenuation, however, could be extremely severe, particularly below 0.5 torr.

The measurements of antenna patterns in the presence of plasma layers are of great interest, and a number of investigators have contributed to the literature on the subject. For example, horn antennas have been dealt with by Cloutier and Bachynski [1] and Jacavanco and Meltz [2]. These plasmas were glass-confined gas discharges created by external excitation and are quite different from the plasmas caused by RF breakdown of the radiating antenna itself. For the latter case antenna patterns have been measured by Chown *et al.* [3] and Yee [4] for traveling wave antennas.

In this experimental study a pulsed microwave signal is transmitted from a slot antenna in the presence of an RF breakdown plasma just outside the aperture. This plasma is represented by a wide variety of luminous configurations which depend upon breakdown power and gas pressure. The radiation patterns in the E and H planes are examined under breakdown conditions. The breakdown plasma was photographed routinely as were the CRO traces of transmitted and reflected breakdown pulses. The spectral content of the transmitted breakdown pulse was monitored by a spectrum analyzer. For further details of this study the reader is referred to a recent report [5].

Experimental Arrangement

The patterns were measured at different times during the active breakdown sheath and during the sheath afterglow by using a separate pulsed signal with a variable delay. The frequency of this signal ($f=9.71$ or 10.00 GHz) was close enough to that of the breakdown signal ($f=9.39$ GHz) so that the plasma properties appear to be nearly the same for the two signals.

Fig. 1 shows the experimental arrangement. An x–y recorder recorded the antenna radiation patterns. A precision potentiometer converted the angular displacement of the boom into a voltage which served as an x input, and the power picked up by the receiving horn served as the y input. It was found that by carefully grinding both the ground plane and the edge of the plexiglass hemisphere and sparingly applying high-vacuum grease between the two surfaces the hemisphere could be pumped down to a pressure of less than 10^{-5} torr. The air was bled through a drying unit before entering into a chamber consisting mainly of a liquid N_2 cold trap from which the gas finally was introduced into the hemisphere.

Results

Antenna patterns with and without the plexiglass hemisphere were recorded under "cold case" conditions, i.e., no breakdown. The main effect of the hemisphere is an overall attenuation (≈ 1.5 dB) which is reasonably independent of angle. Some of the ripples on the patterns, observed both with and without breakdown, are believed (at least partly) to be caused by reflections from the ground-plane peripheral edges.

The breakdown plasma sheath becomes more restricted with more marked boundaries the higher the gas pressure, and a rather small portion of the total aperture area is occupied by the luminous plasma for the lowest powers. The high-power breakdown sheath leads to an increase in reflection after breakdown occurs; the low-power plasma configurations result in markedly less reflection than in the cold case, when 14 percent of the incident power is reflected for 9.39 GHz. This phenomenon took place both in air and helium over a wide range of pressures. Manifestation of breakdown existed down to a pressure of 0.06 torr. At low pressures the oval-shaped luminous sheath extended considerably beyond the width of the aperture in the E-field direction and had rather diffuse boundaries in both the vertical and lateral extension.

It was always found that attenuation was less severe immediately following breakdown than toward the end of the breakdown pulse. Sometimes more power is transmitted during the immediate afterglow of the breakdown plasma than in the cold case. This phenomenon was observed in air and helium and is still unresolved because the increment in power is often more than can be accounted for even by assuming an afterglow plasma which gives rise to a perfect antenna match. This effect is power and pressure dependent. The increase in power appeared to occur after some contamination of the gas had taken place. Further investigations of this phenomenon are clearly desirable.

In air a magnetron furnished the breakdown pulse which was about 2 μs long with a maximum peak power available of about 26 kW. A typical E-plane pattern in air is shown in Fig. 2(a). The cold-case pattern has a dip at about 75 degrees to one side. This dip is still present under breakdown conditions. However, it is less pronounced than without breakdown. No distortion of any significance is in evidence on E-plane patterns for all the pressures and powers covered in this investigation. The corresponding H-plane pattern is shown in Fig. 2(b). The attenuation is most severe at broadside during breakdown leading to an increased beamwidth. This feature was observed in both air and helium. There are no significant pattern distortions.

A few samples of shapes of the transmitted pulses are shown in Fig. 3. The magnetron breakdown pulse without breakdown, seen on the upper trace, has a rise time of about 100 ns. For $p \leq 0.10$ torr, full peak power (25 kW) is needed to cause breakdown. For $p \geq 0.15$ torr, breakdown occurs at powers less than the full peak value leading to a spiked configuration of the transmitted pulse. At 100-torr, breakdown does not cause an abrupt "blackout" but rather a gradual increase in pulse attenuation. The very narrow pulse in Fig. 3 was typical of the middle pressure range, where minimum breakdown powers are needed. Such a pulse exhibits a wide power spectrum which sometimes overlaps the spectrum of the probing signal. By routinely monitoring the receiver output with a spectrum analyzer, the contribution from

Manuscript received November 21, 1968. This work was supported by the U.S. Air Force Cambridge Research Laboratories under Contract AF-19(628)-5718.